forum acusticum 2023

EFFECT OF THE INCIDENCE ANGLE OF THE FLOW ON THE ACOUSTIC DIPOLAR RADIATION OF RECTANGULAR CYLINDERS

Louise Chiocchetti[1*]   **David Marx**[1]   **Florent Margnat**[1]   **Vincent Valeau**[1]

[1] Institut Pprime, CNRS-Université de Poitiers - ENSMA,
B17, 6 rue Marcel Doré, 86073 Poitiers, France

ABSTRACT

This study focuses on the noise produced by cylinder-flow interactions. The aerodynamic noise is established when the instabilities in the shear layer lead to periodic vortex shedding. This results in a tonal noise called "aeolian tone". For a rectangular cylinder with no incidence, the sources of noise are located along the spanwise direction. They have a dipolar directivity, orthogonal to the flow. However, when the incidence of the flow varies, the orientation of the dipoles changes. This phenomenon is investigated experimentally in the test section of an anechoic wind-tunnel, with an array of microphones placed orthogonally to the cylinder. The rectangular cylinders studied have two different aspect ratios: AR=1 and AR=2, for Reynolds numbers between 2 000 and 23 000. A beamforming-based method is used to recover the dipolar angles from the microphones data. For the two cylinders, the dipole tilts similarly when changing the flow incidence angle. These results confirm numerical predictions of the sound directivity based on Curle's solution, for a compact source using the drag and lift force fluctuations.

Keywords: *rectangular cylinder, incidence angle, dipole, directivity*

1. INTRODUCTION

Research on the aerodynamic noise emitted by a cylinder in a flow has been conducted extensively [1]. However, the majority of studies on this field focused on circular cross-sections [2]. Concerning rectangular cross-sections, experimental studies have shown variations in the wake properties due to geometrical characteristics, making parameters such as the aspect ratio [3],

the incidence angle [4–6], and the sharpness [7] crucial in the flow analysis. Specifically, the contribution of the drag dipole is enhanced compared to circular cylinder, and the separation points are fixed on corners. In the absence of incidence of the incoming flow, the resulting sound has a dipolar directivity that is orthogonal to both the cylinder and the flow.

Physically, a flow impinging on a rectangular cylinder separates from the upstream corners (except at really low Re). A vortex is shed from one side of the object, which induces a negative pressure pulse on this side, and a positive pressure pulse on the other side. Vortices are then shed alternately from the two sides of the cylinder, and this induces sound pressure waves from the two sides. This sound is established as the wake becomes unsteady, namely when $Re > 40$ [8]. The transition between 2D-3D wake is observed between $200 < Re < 300$. As the value of Re increases, turbulence appears closer to the cylinder, until it extends to the shear layer (around $Re = 3,5.10^5$).

A previous paper predicted numerically the acoustic directivity of a rotating rectangle for $Re = 200$, using Curle's analogy [9] (with an aspect ratio of 4). This paper exhibited the influence of the flow incidence on the induced-dipole orientation. However, the experimental validation of this model remains unexplored.

The present study aims to investigate experimentally the impact of flow incidence on the induced-dipole directivity for two distinct aspect ratios, AR=1 (square cross-section) and AR=2 (rectangular cross-section), within the test section of an anechoic wind tunnel. In order to allow an accurate estimation of the dipole orientation, a planar array approximately orthogonal to the cylinder is used. The experiments are performed between $2\,000 < Re < 23\,000$: the wake is turbulent, but the boundary layer separation is laminar. The observed results are compared with numerical predictions.

The paper is structured as follows. In Section 2, the experimental setup and the method of data processing are exposed. Then, the numerical model that provides results at low-Reynolds number is described in Section 3. The effect of

10th Convention of the European Acoustics Association
Turin, Italy • 11th – 15th September 2023 • Politecnico di Torino

4551

the angle of attack and the Reynolds number are discussed and compared to numerical predictions in Section 4. Finally, the contribution and limitations of this work are argued in Section 5.

2. EXPERIMENTAL METHOD

2.1 Experimental set-up

The series of experiments presented in this paper was conducted in the anechoic wind tunnel BETI of the Pprime Institute. The anechoic room has a volume of $90\,\mathrm{m}^3$ and a cutoff frequency of $200\,\mathrm{Hz}$. The dimensions of the nozzle are $(0.7\times0.7)\mathrm{m}^2$, and the distance between the nozzle and the collector is $1.5\,\mathrm{m}$ (Fig. 1). The part of the array used for this paper is made of 256 MEMs microphones attached to 16 aluminium bars oriented towards X. The microphones periodicity are $\Delta x \approx 7\,\mathrm{cm}$ and $\Delta y \approx 8.5\,\mathrm{cm}$ The array is based on the MegaMicros system [10].

The studied cylinder, made of steel, is positioned vertically within the test section, at X = $36.5\,\mathrm{cm}$ from the nozzle, centred with respect to the nozzle in the Y direction. It is nested on two metal supports at the top and bottom at Z = $55\,\mathrm{cm}$ and Z = $-55\,\mathrm{cm}$ respectively. The cylinder protrudes beyond the top side array. The supports are covered with foam to prevent unwanted diffraction phenomena.
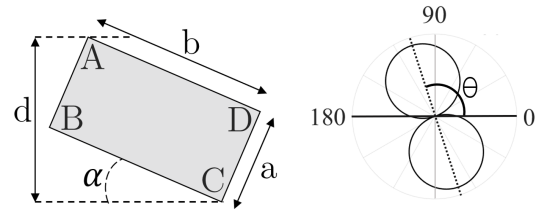
The parameters of the experiments are detailed in Table 1, and the notations are specified in Fig. 2: the measurements are performed every two degrees for the angle of attack α, for a recording time of 5 seconds, at the sampling frequency F_e = $50\,\mathrm{kHz}$. For the experimental determination of the angle of attack, a half disk is positioned underneath the cylinder, with the angles noted (every $2°$ from $0°$ to $180°$). A needle is welded to the down part of the cylinder, which aligns with the angles indicated on the half disk. The angle θ is the one between the induced-dipole axis and the direction of the incoming flow ($\theta = 90°$ for $\alpha = 0°$).
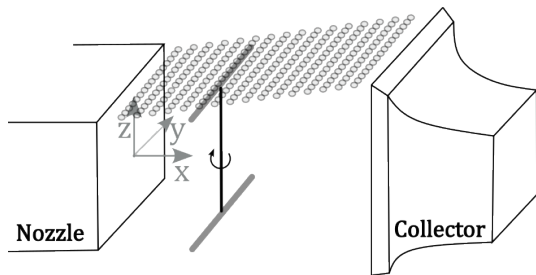
Figure 1: Diagram of the test section in the BETI anechoic wind-tunnel: the nozzle is on the left, the cylinder in the middle, fixed to two metal supports, and the collector on the right. The flows goes from the left to the right side.

Table 1 – Cylinder's section shape and velocities.

Section	Square d=7mm	Rectangle d=6x11,5mm
$U_\infty(m/s)$	10,15,30,50	20,30,50
$\alpha(°)$	$0 \mapsto 90$	$0 \mapsto 90$

Figure 2: Configuration and notations for the experiment of a rectangular cylinder at incidence towards a flow. On the left, the top view of a cylinder's cross-section with an angle of incidence α is represented. On the right, the orientation angle θ of the dipole is specified.

2.2 Data processing

The dipole orientation is estimated with a dipole-based beamforming method as proposed in Ref. [11]: after the cross-spectral matrix calculation using the Welch method, beamforming is performed in the frequency domain, at the frequency of the tonal sound, on the XY plane, at $Z = 0\,\mathrm{m}$ (middle of the test section). In this work, a dipolar steering vector is used [12]:

$$\mathbf{E}^{dip,\theta}(r,\omega) = \frac{e^{-i\omega r/c_0}}{4\pi r}\left(\frac{\mathbf{x}_s - \mathbf{x}_m}{r}.\boldsymbol{\xi}_\theta\right) \tag{1}$$

with c_0 being the speed of sound, $\boldsymbol{\xi}_\theta$ a vector oriented on a direction that makes an angle θ with the observer, and $r = |\mathbf{x}_s - \mathbf{x}_m|$ the distance location between the considered microphone and the position of a point describing the scanning domain.

Considering the location of the cylinder, the corresponding scanning point on the grid is known: at this scanning point, the dipole-based beamforming is successively implemented for all possible dipolar orientations $\boldsymbol{\xi}_\theta$ with a precision of $\pm\,0.1°$. The estimated orientation for the dipole is the angle θ that maximises the calculated amplitude at the cylinder location.

3. NUMERICAL MODEL

A hybrid method based on coupling Curle's analogy and IBM (Immersed Boundary Methods) is conducted to predict the orientation of the flow-induced acoustic sources on a cylinder [9]. First, the fluctuation of the aerodynamic force is obtained with a numerical simulation, considering an incompressible, 2D flow. Then, Curle's approach for compact sources uses these fluctuations to estimate the acoustic pressure in the far field.

The acoustic field in the 3D case depends on the energy of the fluctuating forces, and on the span on which this energy is efficiently radiating. Consequently, to predict the acoustic pressure, the fluctuation of aerodynamic forces is first calculated: drag and lift forces F_y and F_x are respectively the streamwise and transverse components of the force applied to the obstacle surface by the fluid.

The mean acoustic intensity at the dominant flow frequency is approximated as follows in the 2D far field:

$$I_a(R, \varphi, f_s) \approx \frac{f_s}{2\rho_0 c_0^2 R} \big[|\hat{F}_x|^2 \cos^2 \varphi + |\hat{F}_y|^2 \sin^2 \varphi \\ + (\hat{F}_x \hat{F}_y^* + \hat{F}_x^* \hat{F}_y) \cos \varphi \sin \varphi \big] \quad (2)$$

where ρ_0 is the density of the air, (R, φ) are the polar coordinates centred on the body with $\varphi = 0$ in the flow direction, f_s the lift fluctuation frequency, * denotes the complex conjugate and

$$\hat{F}_q = \int_{-\infty}^{+\infty} F_q(t) \, e^{-i2\pi f_s t} \, dt \quad (3)$$

is the Fourier mode of F_q corresponding to f_s. Though $|\hat{F}_x|$ is greatly smaller than $|\hat{F}_y|$, especially for symmetric bodies (e.g. square at $0°$ or $45°$ of incidence), it is enough significant to tilt the dipole directivity away from $\theta = 90°$ due to the last term in (2).

For any angle φ, the intensity is calculated using Eqn. (2), and the highest value obtained corresponds to the orientation of the dipole. Finally, the noise radiated by the flow over a rectangular cylinder at $Re = 200$, based on the upstream velocity and the blocking height of the cylinder d, is computed for 10 values of $\alpha \in [0°, 90°]$. The incidence varies while the blockage length and the aspect ratio are maintained constant ($b/a = 1$ and 2): the difference with our experiments is that the size of the cylinder changes for every incidence angle, so that Re based on d is kept constant.

3.1 Square section (AR=1)

As shown from Eqn. (2), the lift and drag fluctuations forces are crucial for determining the tilt angle of the dipole. These fluctuations, computed using the IBM technique, are presented in Fig. 3: the lift fluctuation is plotted as a function of the drag fluctuation, revealing the trajectory of the head of the fluctuation force vector, for one cycle of vortex-shedding.

The configuration looks symmetric with respect to the X-axis when $\alpha = 0°$ and $\alpha = 45°$, which means that the flow is symmetrical. It will be shown in Section 4 that at those incidences, the dipole is in the Y direction ($\theta = 90°$). Though emphasized by the non-orthonormal frame, a shift of orientation is definitively observed at $\alpha = 45°$: before, the loop has a North-west/ South-East orientation, and after, it tilts to a South-West/ North-East orientation. The pattern is the same every $90°$, and this remarkable behaviour is commented in Section 4.1.

3.2 Rectangular section (AR=2)

Fig. 4 presents the same graphs as in Fig. 3, for the rectangular cross-section. Though, several differences are observed. First, the angles where the graph is symmetric are $\alpha = 0°$ and $90°$. Moreover, $90° - \alpha$ and $90° + \alpha$ graphs are symmetrical. The rotation of the rectangle has a pattern repeated every $180°$. Furthermore, the loop crosses itself at $\alpha = 30°$. It will appear later that this angle indicate the moment when the dipole tilts away from the downstream direction to the upstream direction. It can be noticed that for $0° < \alpha \leq 30°$, the loop is oriented North-West/ South-Est. On the contrary, for $30° < \alpha < 90°$, it shifts to a North-Est/ South-West orientation. This behaviour will be linked to the experimental results in Section 4.2.

4. EXPERIMENTAL RESULTS

4.1 Square section (AR=1)

The experiments are shown for $0° < \alpha < 90°$. However, to make sure that the results are reproducible and symmetrical, the experiments have been performed from $\alpha = -45°$. The Strouhal number, based on the blockage section d (see Fig. 2), is calculated for every incidence angle as follows:
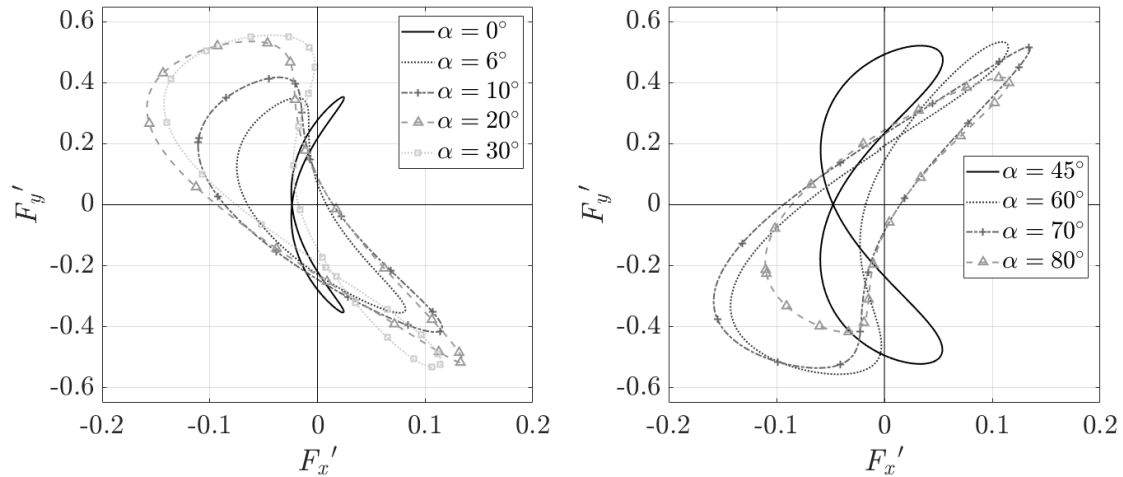
$$St_d = f_s d / U_\infty \quad (4)$$

with f_s the dominant vortex shedding frequency (determined by the first peak of the frequency spectrum).
The Strouhal number is plotted on the upper part of Fig. 5, with the numerical model ($Re = 200$), as a function of the imposed incidence angle. It is found to be maximal $St_{max} = 0, 2$ for the experiments, and $St_{max} \approx 0.22$ for the model. As expected, the graph is symmetrical with respect to $\alpha = 45°$.

At $\alpha = 0°$, St is at its minimum. Then, it increases until the first peak, corresponding to a critical angle α_{cr}, namely the angle when the flow reattaches on the side B-C [13]. This critical angle is dependant on Re, and is reported on Tab. 2: the higher Re is, the lower α_{cr} is observed. On the numerical prediction, there is no critical angle corresponding to α_{cr}, but the tendency between $0° < \alpha < 20°$ is similar.

The dipole orientation θ is sketched as a function of the incidence angle on the bottom part of Fig. 5. The angle θ is determined with a method of dipole-based beamforming (see Section 2.2). The dipole is shown to have a global rotation

10th Convention of the European Acoustics Association
Turin, Italy • 11th – 15th September 2023 • Politecnico di Torino

4553

Figure 3: Lift fluctuation as a function of drag fluctuation over one cycle of vortex shedding, for a square section cylinder (AR=1). On the left: low incidence angles ($0° \leq \alpha \leq 30°$), and on the right: high incidence angles ($45° \leq \alpha \leq 80°$). The values come from the model prediction at $Re = 200$.
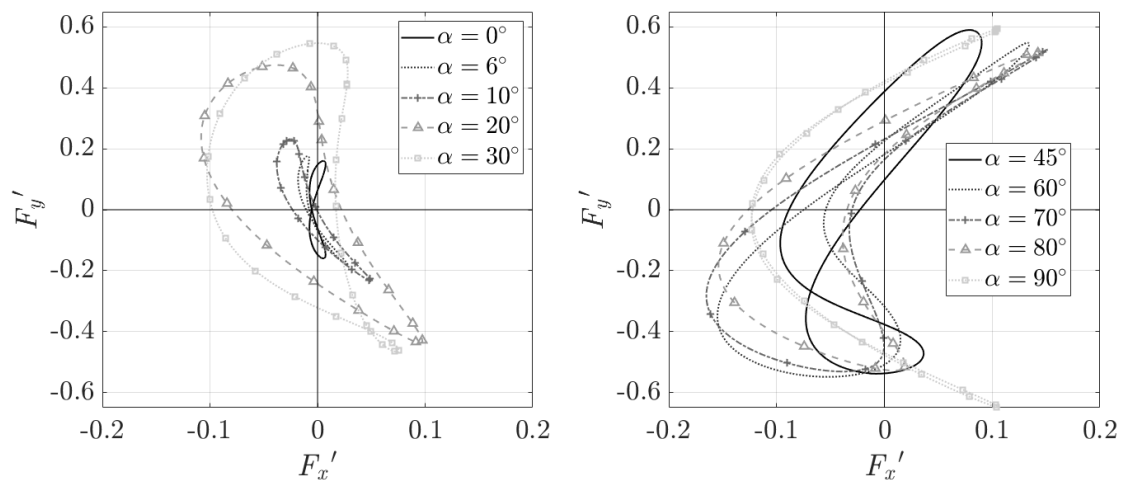
Figure 4: Lift fluctuation as a function of drag fluctuation over one cycle of vortex shedding, for a rectangular section cylinder (AR=2). On the left: low incidence angles ($0° \leq \alpha \leq 30°$), and on the right: high incidence angles ($45° \leq \alpha \leq 90°$). The values come from the model prediction at $Re = 200$.

of $\pm 15°$. The different phases and the corresponding dipole changes are summarised in Tab. 3, where the gradient from grey to black arrows shows the variation of the dipole orientation.

When $\alpha = 0$, the dipole orientation is $\theta = 90°$ and the fluctuating lift and drag forces show perfect symmetry: this is referred to as the subcritical regime [14], where the vortex detachment is also symmetric, on the top and the bottom of the section (the reattachment varies with Re).

As α increases from $0°$ to α_{cr}, the system transitions to a critical regime and the Strouhal number increases very quickly, reaching its maximum at α_{cr} (see Tab. 2). The dipole orientation θ evolves linearly to reach $\theta \approx 80°$. According to [14], when

10th Convention of the European Acoustics Association
Turin, Italy • 11th – 15th September 2023 • Politecnico di Torino

4554

$St \approx 0.2$ is at its maximum ($\alpha = \alpha_{cr}$), the flow detaches at corner B and reattach to the cylinder surface on the B-C face, which induces a huge pressure change on this face: this phase is also named the separation bubble regime. On this same angle $\alpha = \alpha_{cr}$, the stagnation point is getting closer to point B (see Fig. 2) [15], and the dipole tilts away from the flow direction, reaching its maximum (around $\theta \approx 100°$).

In the supercritical regime ($\alpha > \alpha_{cr}$), detachment occurs at the corners A and C of the cylinder, while the stagnation point is located at B. Notably, θ decreases smoothly and gradually until it ultimately reaches 0 for $\alpha = 45°$.

Moreover, the pattern described above is consistent across all measurements conducted at different Reynolds numbers, and the critical angles are the same for the two graphs of Fig. 5 (St and θ).
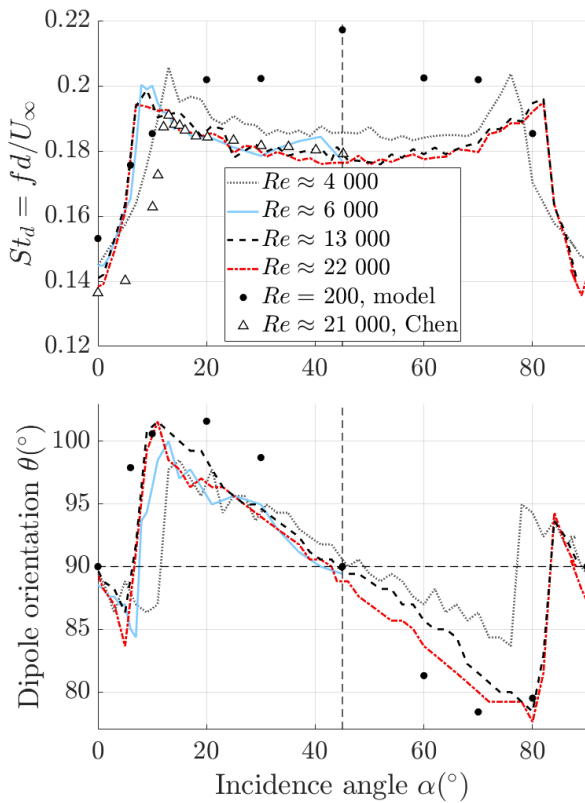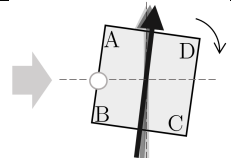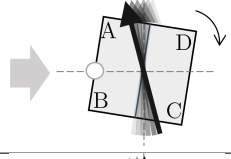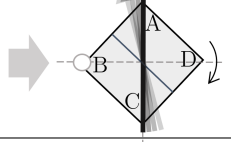

Figure 5: Strouhal number (top) and directivity of the dipole θ (bottom) as a function of the incidence angle α for the square cylinder (AR=1) for several Re. The numerical prediction for low Re number is plotted for qualitative comparison. The St_d curve of [16] is plotted for comparison.

Table 2 – Critical angles observed for each flow velocity.

U_∞ (m/s)	Re	α_{cr} (°)
10	4 000	13
15	6 000	10
30	13 000	9
50	22 000	7

Table 3 – Orientation of the dipole for the different regimes (flow from left to right) for the square section (AR=1). The white point stands for the stagnation point [15], and the arrows (from grey to black) represent the variation of orientation of the dipole.

Regime	Scheme
Subcritical $0° < \alpha < \alpha_{cr}$	
Critical $\alpha = \alpha_{cr}$ (depends on Re)	
Supercritical $\alpha_{cr} < \alpha < 45°$	

The numerical model has been computed at $Re = 200$, in a laminar flow (2D): it cannot be quantitatively compared to the experiments, which are performed in turbulent flow (3D). Though, a qualitative comparison can be done. For the dipole orientation, the curves have the same pattern and maximum values as the experimental curves, however, no tilt appears at the critical angle, but this could be due to the lack of points between $\alpha = 0°$ and $6°$.

4.2 Rectangular section

The following paragraph focuses on the rectangular section, which has been studied for $0° < \alpha < 90°$. However, for the same reason as for the square section, the experiments have also been performed from $\alpha = -10°$. The Strouhal number and the

10th Convention of the European Acoustics Association
Turin, Italy • 11th – 15th September 2023 • Politecnico di Torino

4555

tilt angle α are plotted in Fig. 6, as in Section 4.1. The critical angles are listed in Tab. 5.
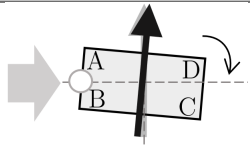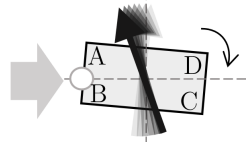
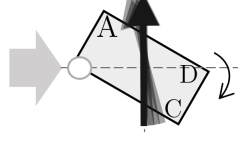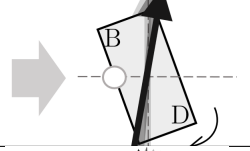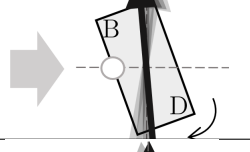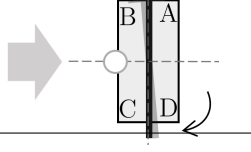The Strouhal number curve has two peak (top Fig. 6), one at $\alpha_{cr,1} = 5°$ and one at $\alpha_{cr,2} = 70°$, for all flow velocities. It can be noticed that the second one is less sharp than the first one. Those two same peaks are observed on the dipole orientation graph also, at the bottom of Fig. 6. The dipole follows linearly the variations of α for $0° < \alpha < 5°$, and tilts away in the opposite direction to reach its maximum angle $\theta \approx 105°$. After α_{cr}, the dipole slowly returns to its initial position, which is observed at $\alpha = 30°$. It is noticed that this position corresponds to when the stagnation point reaches B (see Tab. 4), and also to the change in behaviour of the loops of Fig. 4.

After this, the dipole slowly reaches $\theta = 80°$, and then tilts away to the streamwise direction (at $\alpha = 70°$). Finally, it comes back to the Y direction, for $\alpha = 90°$.
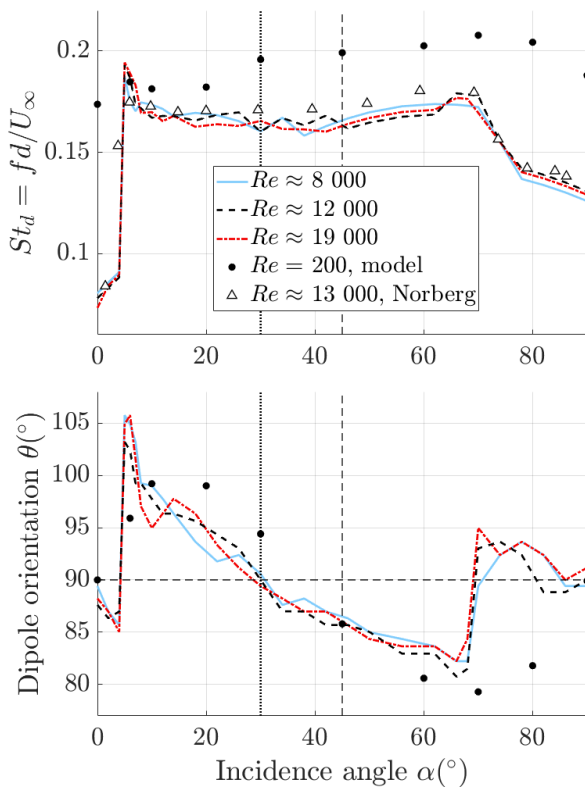
Figure 6: Strouhal number (top) and directivity of the dipole θ (bottom) as a function of the incidence angle α for the rectangle cylinder (AR=2) for several Re. The numerical prediction for low Re number is plotted for qualitative comparison. The St_d curve of [17] is plotted for comparison.

Table 4 – Orientation of the dipole for the different regimes (flow from left to right) for the rectangular section (AR=2). The white point stands for the stagnation point [18], and the arrows represent the variation of orientation of the dipole.

Regime	Scheme
Subcritical $0° \leq \alpha \leq \alpha_{cr,1}$	
Critical $\alpha = \alpha_{cr,1}$ (depends on Re)	
Supercritical $\alpha_{cr,1} \leq \alpha \leq 30°$	
Supercritical $30° \leq \alpha \leq \alpha_{cr,2}$	
Critical $\alpha = \alpha_{cr,2}$	
Subcritical $\alpha_{cr,2} \leq \alpha \leq 90°$	

The first tilt ($\Delta\theta_1 \approx 20°$) is larger than the second one ($\Delta\theta_2 \approx 10°$). The behaviour of the acoustic dipole when the incidence angle varies is summarised in Tab. 4.

Finally, the rectangle section is quite similar to the square one, except there are two different critical angles, because of the fact that the stagnation point is moving slower from A to B than from B to C, given the different lengths.

Table 5 – Critical angles observed for each flow velocity.

U_∞ (m/s)	Re	$\alpha_{cr,1}$ (°)	$\alpha_{cr,2}$ (°)
20	8 000	5	70
30	12 000	5	70
50	19 000	5	70

5. CONCLUSION

First, this study confirmed a strong correlation between the dipole orientation variations, aerodynamic force fluctuations, and the stagnation point position on the cylinder. Therefore, it is very sensitive to small changes in the incidence of the flow.

Furthermore, the pattern of θ variations is observed to be similar for any Reynolds numbers and any aspect ratios. Especially, θ is following the angle of attack until a certain critical angle and then tilts away from the flow direction until the separation point reaches the next corner of the cylinder section (referred to as B here).

Finally, the 2D, low-Re model shows qualitative variations of the dipole angle, which are in very good agreement with the measured trends in the 3D, sub-critical cases. This suggests that the dipole orientation can be explained by 2D dynamics, and is insensitive to the spanwise coherence decay of the source field [19].

In terms of prospects, it would be interesting to get numerical and experimental data with comparable Reynolds numbers, to be able to quantitatively compare our results with each other. Those experiments could also be performed with cylinders of different sharpness and materials.

6. ACKNOWLEDGEMENTS

7. REFERENCES

[1] W. K. Blake, "Dipole Sound From Cylinders," in *Mechanics of Flow-Induced Sound and Vibration, Volume 1*, pp. 251–322, Elsevier, 2017. DOI: 10.1016/B978-0-12-809273-6.00004-X.

[2] J.H Gerrard, "Measurements of the sound from circular cylinders in an air stream," *Proc. Phys. Soc.*, vol. 68, no. 453, 1955.

[3] A. Inasawa, M. Asai, and T. Nakano, "Sound generation in the flow behind a rectangular cylinder of various aspect ratios at low Mach numbers," *Computers & Fluids*, vol. 82, pp. 148–157, 2013.

[4] Tamotsu Igarashi, "Characteristics of the flow around a square prism," *Bulletin of JSME*, vol. 27, no. 231, 1984.

[5] Hajime Fujita, Wei Sha, Hiroshi Furutani, and Hideaki Suzuki, "Experimental investigations and prediction of aerodynamic sound generated from square cylinders," *4th AIAA/CEAS aeroacoustics conference*, p. 2369, 1998.

[6] Anna Mueller, *Large Eddy Simulation of cross-flow around a square rod at incidence with application to tonal noise prediction*. PhD thesis, University of Twente, Twente, 2011.

[7] L. Carassale, A. Freda, and M. Marrè-Brunenghi, "Experimental investigation on the aerodynamic behavior of square cylinders with rounded corners," *Journal of Fluids and Structures*, vol. 44, pp. 195–204, 2014.

[8] W. J. G. S. Pinto and F. Margnat, "Influence of cylinder breadth and shape on the onset of flow unsteadiness and the aeolian tone level," *Computers & Fluids*, vol. 228, p. 105067, 2021.

[9] F. Margnat, "Hybrid prediction of the aerodynamic noise radiated by a rectangular cylinder at incidence," *Computers & Fluids*, vol. 109, pp. 13–26, 2015.

[10] C. Vanwynsberghe, R. Marchiano, F. Ollivier, P. Challande, H. Moingeon, and J. Marchal, "Design and implementation of a multi-octave-band audio camera for realtime diagnosis," *Applied Acoustics*, vol. 89, pp. 281–287, 2015.

[11] J. Gao, H. Wu, and W. Jiang, "Dipole-based beamforming method for locating dipole sources with unknown orientations in three-dimensional domains," *The Journal of the Acoustical Society of America*, vol. 147, no. 1, pp. 125–136, 2020.

[12] R. Porteous, Z. Prime, C. Doolan, D. Moreau, and V. Valeau, "Three-dimensional beamforming of dipolar aeroacoustic sources," *Journal of Sound and Vibration*, vol. 355, pp. 117–134, 2015.

[13] H. Dong, L. Chen, X. Du, L. Fang, and X. Jin, "Effects of corner chamfers on the extreme pressures on a square cylinder at incidence to a uniform flow," *Computers & Fluids*, vol. 244, p. 105539, 2022.

[14] R. Huang, B. Lin, and S. Yen, "Time-averaged topological flow patterns and their influence on vortex shedding of a square cylinder in crossflow at incidence," *Journal of Fluids and Structures*, vol. 26, no. 3, pp. 406–429, 2010.

[15] D.-H. Yoon, K.-S. Yang, and C.-B. Choi, "Flow past a square cylinder with an angle of incidence," *Physics of Fluids*, vol. 22, no. 4, p. 043603, 2010.

[16] Jerry M. Chen and Chia-Hung Liu, "Vortex shedding and surface pressures on a square cylinder at incidence to a uniform air stream," *International Journal of Heat and Fluid Flow*, vol. 20, no. 6, pp. 592–597, 1999.

[17] C. Norberg, "Flow around rectangular cylinders: pressure forces and wake frequencies," *Journal of Wind Engineering and Industrial Aerodynamics*, pp. 187–196, 1993.

[18] M. Matsumoto, "Vortex shedding of bluff bodies: a review," *Journal of Fluids and Structures*, vol. 13, pp. 791–811, 1999.

[19] F. Margnat, W. J. Gonçalves da Silva Pinto, and C. Noûs, "Cylinder aeroacoustics: experimental study of the influence of cross-section shape on spanwise coherence length," *Acta Acustica*, vol. 7, p. 4, 2023.